Top Catal (2008) 51:133–145
DOI 10.1007/s11244-008-9126-8

ORIGINAL PAPER

Autothermal Reforming of Methane with Integrated CO_2 Capture in a Novel Fluidized Bed Membrane Reactor. Part 1: Experimental Demonstration

F. Gallucci · M. Van Sint Annaland · J. A. M. Kuipers

Published online: 24 October 2008

Abstract Two fluidized bed membrane reactor concepts for hydrogen production via autothermal reforming of methane with integrated CO_2 capture are proposed. Ultra-pure hydrogen is obtained via hydrogen perm-selective Pd-based membranes, while the required reaction energy is supplied by oxidizing part of the CH_4 in situ in the methane combustion configuration or by combusting part of the permeated H_2 in the hydrogen combustion configuration (oxidative sweeping). In this first part, the technical feasibility of the two concepts has been studied experimentally, investigating the reactor performance (CH_4 conversion, CO selectivity, H_2 production and H_2 yield) at different operating conditions. A more detailed comparison of the performance of the two proposed reactor concepts is carried out with a simulation study and is presented in the second part of this work.

Keywords Membrane fluidized bed · Methane steam reforming · Autothermal reforming · Hydrogen · Membrane reactor

1 Introduction

On site production of ultra-pure hydrogen for use in downstream Polymer Electrolyte Membrane Fuel Cells (PEMFC) for small or medium scale applications has gained increasing interest in recent years. On an industrial scale, most of the hydrogen is currently produced via steam reforming of methane (SRM). The traditional SRM process consists of feed gas preheating and pre-treatment (such as hydrodesulphurisation), primary and secondary reformers (often multi-tubular fixed-bed reactors) and high and low temperature shift converters, CO_2 removal and methanation units. Often a PSA (Pressure Swing Adsorption) unit is used to achieve the desired hydrogen purity. In view of thermodynamic limitations and the high endothermicity of steam reforming, heat transfer at high temperatures (850–950 °C) is required, where excess of steam is used to avoid carbon deposition (typical feed H_2O/CH_4 molar ratios 2–5) [1, 2]. For the production of ultra-pure hydrogen for small scale application, this route is not preferred because of the large number of process units with complex heat integration and the associated uneconomical downscaling. A high degree of process integration and process intensification can be accomplished by integrating hydrogen perm-selective membranes in the steam reformer [3, 4]. Via the integration of hydrogen perm-selective membranes, the number of process units can be strongly decreased and the total required reactor volume can be largely reduced, while higher methane conversions and hydrogen yields beyond thermodynamic equilibrium limitations can be achieved, at lower temperatures and with higher overall energy efficiencies [5–12].

Steam reforming is a highly endothermic process at elevated temperatures and requires costly external high temperature heat exchange equipment of expensive non-adiabatic reactors in order to supply the required reaction energy, which is very energy inefficient for small scale applications and adds to the complexity of the system [13, 14]. Autothermal operation yields without external or internal heat exchange can be accomplished through a combination of steam reforming and oxidation, in two conceptually different ways. On the one hand, by co-feeding air or pure oxygen, part of the methane can be

F. Gallucci · M. Van Sint Annaland (✉) · J. A. M. Kuipers
Fundamentals of Chemical Reaction Engineering Group, Faculty of Science and Technology, IMPACT, University of Twente, P.O. Box 217, 7500 AE Enschede, The Netherlands
e-mail: m.vansintannaland@tnw.utwente.nl

oxidised to generate the required energy for the steam reforming in situ (methane combustion concept). Use of pure oxygen avoids nitrogen dilution, which keeps the required reactor volume small and allows integrating CO_2 capture (circumventing costly CO_2/N_2 separation), but requires an expensive cryogenic air distillation unit. This could be circumvented by integrating the O_2/N_2 separation inside the reactor by incorporating oxygen perm-selective (e.g. perovskite type) membranes in the reactor [15], however, oxygen perm-selective membranes still require further development concerning their mechanical and chemical stability. On the other hand, part of the produced hydrogen can be oxidised to supply the reaction energy (hydrogen combustion concept). This can be accomplished both directly, via recycling part of the hydrogen combusted with air, and indirectly, e.g. via oxidative sweeping (i.e. sweeping with air) on the permeate side of the hydrogen perm-selective membranes, which also allows complete integration of CO_2 capture but circumvents the use of oxygen perm-selective membranes. Process concepts with integrated CO_2 capture will become increasingly interesting anticipating increasing costs associated with anthropogenic CO_2 emissions. Whether it is beneficial to provide the required energy via burning CH_4 with air using a consecutive separate CO_2/N_2 step or via burning CH_4 with pure O_2 with an ASU (Air Separation Unit) or burning H_2 obtained via the membranes, remains an overall economical evaluation. In this work, these two different process concepts with integrated CO_2 capture are evaluated with experiments to give a proof of principle (Part 1) and compared on the basis of a modelling study (Part 2).

The conceptual feasibility of Packed Bed Membrane Reactors (PBMR) for the autothermal reforming of methane has been investigated by many research groups [16, 17]. Tiemersma et al. used a detailed numerical simulation study with a 2D reactor model and evaluated different operation modes [16]. In principle, high energy efficiencies could be achieved with a PBMR for autothermal methane reforming, but very large undesired temperature gradients along the reactor were observed when the reactor was operated adiabatically, which are detrimental for membrane stability. In fact, Ioannides and Verykios [18] experimentally measured large temperature excursions close to the reactor inlet carrying out ATR in a packed-bed reactor, which they attributed to the higher reaction rate of methane oxidation compared to the SRM. These observations have also been supported by simulations using 1D non-isothermal models [17, 19]. Moreover, mass transfer limitations from the catalyst bed to the membrane surface (also referred to as concentration polarization) as a result of the selective H_2 removal, were found to be quite important, especially for membranes with the commercially required high membrane permeability. Concentration polarization (and the associated losses in reactor performance) can only be avoided by selecting a small membrane tube diameter, while pressure drop restrictions limit the minimum size of the catalyst particles (resulting in low particle effectiveness factors), thus leading to undesired, small tube diameter over particle diameter ratios. All these disadvantages can be overcome by using fluidized beds, with which heat and mass transfer rates can be greatly improved compared to what can be maximally achieved with fixed beds, at much lower pressure drops. Recently, Patil et al. [15] indeed demonstrated the absence of temperature gradients and mass transfer limitations to the membrane surface in a Fluidized Bed Membrane Reactor (FBMR) for methane steam reforming. Also Boyd et al. [20], Abashar and Elnashaie [21] and Chen et al. [22] showed the good performance of FBMRs for autothermal reforming of methane without problems associated with mass transfer limitations or temperature profiles.

In this work, the two different fluidized bed membrane reactor concepts for autothermal methane reforming with integrated CO_2 capture are studied, the first concept is based on methane combustion (extending the work by Patil et al. [15]) and the second concept is based on hydrogen combustion (novel concept). In Part 1, the technical feasibility of the two concepts are assessed with dedicated experiments giving a proof of concept. First, the fluidized bed membrane reactor concepts are described in more detail and the experimental set-up is outlined. Subsequently, the experimental results on the two concepts are described and discussed. In Part 2 the reactor performance of the two concepts is compared over a wide range of operating conditions using simulations.

2 Fluidized Membrane Reactor Concepts

The two fluidized bed membrane reactor concepts are schematically depicted in Fig. 1. Figure 1a shows the methane combustion configuration. Hydrogen perm-selective membranes are integrated in a fluidized reforming/shift top section where ultra-pure H_2 is extracted and the energy required for the steam reforming is supplied via in situ methane oxidation in a separate fluidized bottom section, where oxygen is selectively fed to the methane/steam feed via oxygen perm-selective membranes. Two different sections are required because metallic Pd-based membranes for selective H_2 extraction can only be operated below typically 700 °C because of membrane stability, while acceptable O_2 fluxes through available perovskite-type O_2 perm-selective membranes can only be realized above 900–1000 °C (see also Patil et al. [15]). Alternatively, air or pure oxygen could be fed directly to the top section, in which case, however, air separation or CO_2

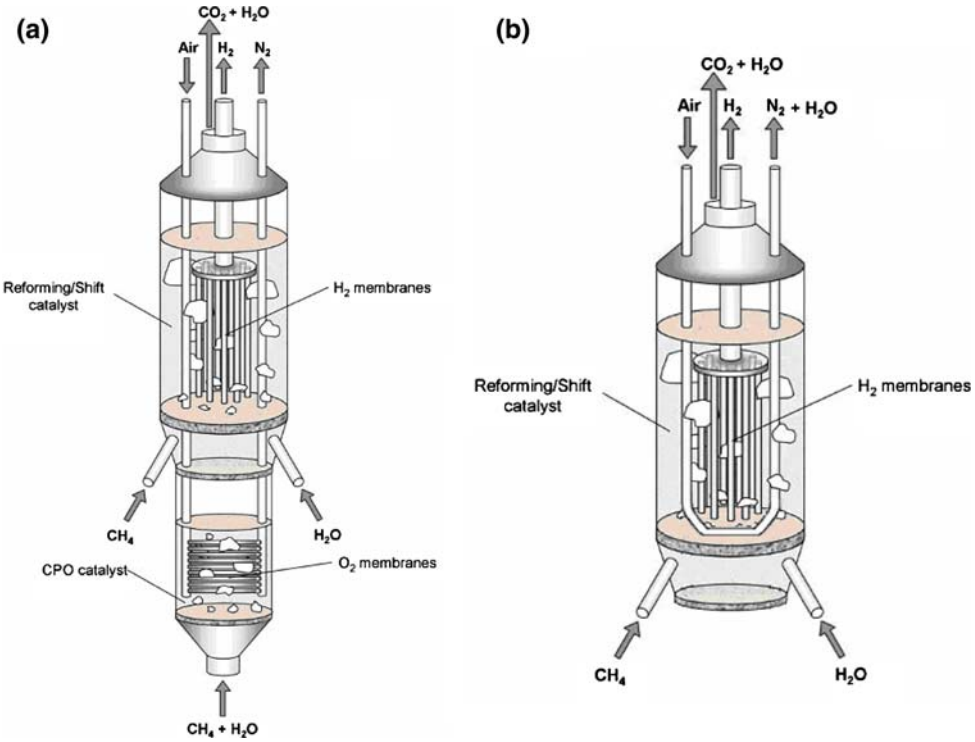

Fig. 1 Schematic representation of the two fluidized membrane reactor concepts for autothermal methane reforming with integrated CO_2 capture. **a** Methane combustion configuration. **b** Hydrogen combustion configuration. Reprinted from Patil et al. [15], with permission from Elsevier

capture is no longer integrated in the reactor. In the oxidation section, CH_4 is partially oxidized in order to achieve the high temperatures required for O_2 permeation through the perovskite membranes and to simultaneously preheat part of the CH_4/steam feed. The preheated feed is mixed with additional CH_4 and steam and fed to the reforming/shift section, where CH_4 is completely converted to CO, CO_2 and H_2 because of the selective H_2 extraction through the Pd membranes which shifts the methane steam reforming. H_2 extraction can be achieved by using dead-end Pd membranes and applying a vacuum on the permeate side. Alternatively, a sweep gas (such as H_2O) could be used, but the decrease in membrane area due to the increased driving force should outweigh the additional costs for separating H_2 from the sweep gas. Overall autothermal operation can be achieved by tuning the overall CH_4, O_2 and steam fed to the reactor. The distinct advantage of this reactor concept is that the temperatures in both sections can be controlled independently by selecting the proper ratio of CH_4/H_2O fed at the oxidation and reforming/shift sections, while maintaining overall autothermal operation with optimal energy efficiency.

In Fig. 1b the novel hydrogen combustion configuration is shown, where the energy for steam reforming is delivered via burning part of the produced hydrogen. This configuration consists of only one fluidized bed section, where two types of hydrogen perm-selective membranes are incorporated: dead-end Pd-based membranes to recover ultra-pure H_2 by applying a vacuum on the permeate side (similar to the ones used in the methane combustion configuration) and U-shaped Pd-based membranes with oxidative sweeping, by feeding air to the permeate side to burn the permeated hydrogen. The hydrogen combustion configuration has the clear advantage that only one section is required, circumventing the need for a (costly) high temperature bottom section. On the other hand, in the methane combustion configuration steam is produced in situ, which enhances the CO conversion. Moreover, in the hydrogen combustion configuration, part of the expensive Pd-based membranes are used to burn part of the produced hydrogen, while for the methane combustion configuration further development of oxygen perm-selective membranes (esp. the mechanical and chemical stability) is essential. In this paper the technical feasibility of the two reactor concepts for autothermal reforming of methane is investigated experimentally. The experimental results for the two concepts will be interpreted with a simplified model. In the second part of this work, a more detailed reactor model will be used to compare the performance of the two reactor concepts as a function of the operating conditions.

3 Experimental Setup

In order to assess the technical feasibility of both concepts, a fluidized bed membrane reactor was constructed of 10 cm diameter and 60 cm height, equipped with 10 cylindrical dead-end Pd-based membranes, connected via a

Fig. 2 Pictures of the membrane assembly (**a**) and the fluidized membrane module (**b**)

tree structure to the permeate side of the reactor, and 2 U-shaped cylindrical Pd-based membranes (see Fig. 2). For testing the methane combustion configuration, the lines to and from the U-shaped membranes were closed, while the testing of the hydrogen combustion configuration was carried out with only one of the U-shaped membranes, using the second one as a spare, to which could be switched without opening the reactor (but this provision turned out to be abundant). The dead-end and U-shaped Pd-based membranes used in the reactor have been procured from REB Research and Consulting, Ferndale, USA. Both membrane types consist of metal tube reinforced with Inconel with on both sides a thin layer of Pd. The dead-end membranes are 3.2 mm in diameter and 20 cm in length with a Pd layer of 4–5 μm thickness on the inside and outside. The U-shaped membranes have dimensions: 3.2 mm diameter and 41 cm length, with a Pd layer thickness of 1.5 and 0.3 μm on the outside and inside, respectively. The methane combustion configuration was simulated by feeding air directly to the fluidized bed. At the moment, problems concerning the mechanical and chemical stability and sealing of perovskite type membranes prohibits testing the methane combustion configuration with completely integrated air separation.

The process flow diagram for the pilot plant set-up is depicted in Fig. 3. The setup consists of three sections, a feed section, a reactor section and an analysis section. The feed section consists of the feed gases supply from gas cylinders (N_2, H_2, CH_4 and Air) and mass flow controllers to set the desired flow rate and gas composition. All gas supply lines are additionally protected with pneumatically

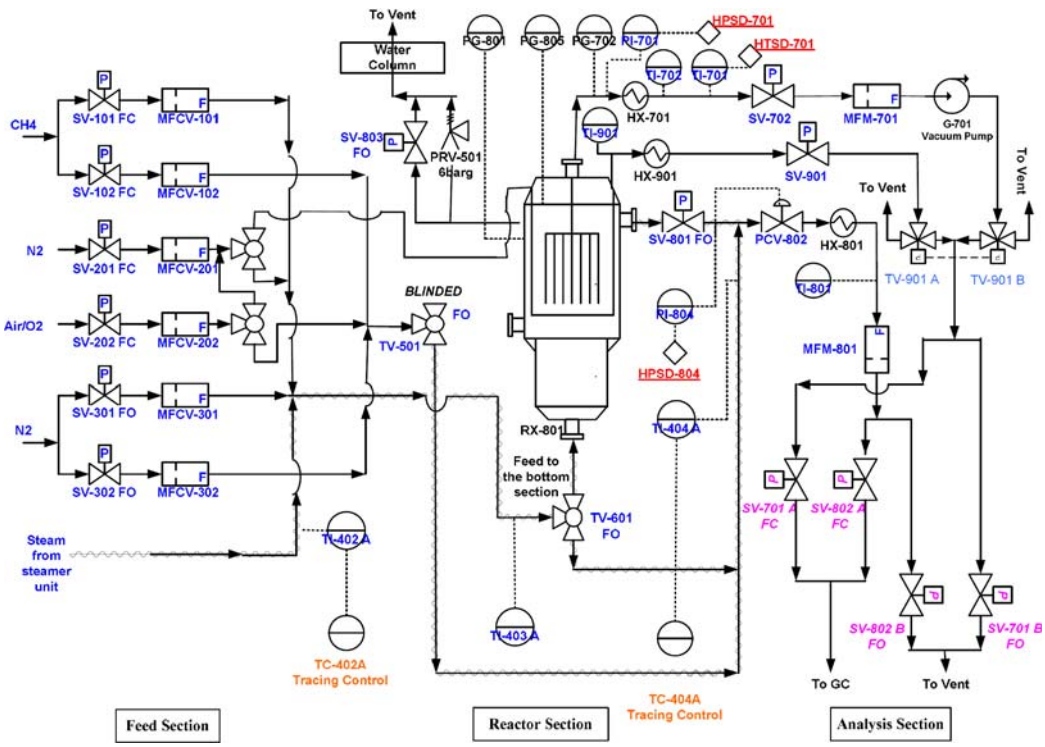

Displayed Text	*Description*
FL-801	Filter
G-701	Vacuum Pump
GC	Gas Chromatograph
HX	Steam Generator/ Cooler
HPSD	High Pressure Shut Down
HTSD	High Temperature Shut Down
MFCV	Mass Flow Controller
MFM	Mass Flow Meter
PG	Pressure Gauge
PI	Pressure Indicator
RX	Reactor
SV	Safe valve
TC	Temperature Controller
TI	Temperature Indicator

Fig. 3 Process flow diagram of the pilot plant set-up

operated shut-off valves to cut-off gas supply in case of an emergency shutdown. For the steam generation a HPLC pump is used to feed a precise amount of demineralised water into an electrical furnace that generates steam. The steam supply lines and the reactor exhaust lines are insulated and covered with electrical tracing to maintain the temperature sufficiently high (~200 °C) to avoid water condensation and pressure fluctuations in the reactor due to droplet formation.

The fluidized bed membrane reactor is heated using three electrical furnaces in order to overcome unavoidable heat losses. The reforming catalyst was specially prepared by Shell Global Solutions International b.v. and is a highly active noble metal-based CPO catalyst. Two commercial Ni-based catalysts were tested and severe coking was found with these catalysts at the operating conditions investigated in this work in strong contrast with the noble metal-based catalyst. The catalyst particles (sieved to 50–75 μm) were largely diluted with alumina particles (104 μm) (using 50 g catalyst and 1.4 kg alumina) to provide sufficient bed height for complete immersion of the Pd membranes in the fluidized suspension. With the selected particle sizes, particle segregation in the fluidized mixture was found to be minimal (concluded from separate experiments in a small glass fluidized bed at atmospheric conditions). The alumina particles were procured from Aldrich (activated neutral Brockmann type of 150 mesh size) and treated at 900 °C for 24 h (to convert the γ-phase into the α-phase and reduce the surface area and acidity). By conducting experiments in the pilot plant without CPO catalyst and with and without inert particles it was ensured that the contribution of gas phase reactions is negligible and that the reactor metal tube and inert particles do not exhibit catalytic activity. Moreover, with experiments in which the CPO catalyst amount was varied, it was excluded that reaction kinetic limitations restricted the methane conversion.

The reactor feed (using a three-way valve to bypass the reactor), reactor exhaust (retentate), product H_2 (permeate) or U-tube exhaust streams are sampled and their composition analyzed using an IR analyzer, with which the H_2, CO, CO_2 and CH_4 content is measured, or a micro-GC (Varian CP-4900) equipped with two molsieve (5 Å) columns and one Poraplot Q column. One of the molsieve columns is used to detect O_2, N_2, CH_4 and CO, while the other is used to detect H_2 or He. The Poraplot Q is used to measure CO_2 and traces of H_2O. For more details on the experimental set-up and experimental results (including details on experimental errors) for methane steam reforming conditions (i.e. without methane combustion or hydrogen combustion), the interested reader is referred to Patil [23]. The experimental error was always within 2%, based on the overall carbon balance. Before discussing in detail the experimental results for the methane and hydrogen combustion configurations and the effect of different operating conditions on the reactor performance, the hydrogen permeability of the dead-end and U-shape Pd-membranes is discussed.

4 Results and Discussion

4.1 Hydrogen Permeability

Based on extensive membrane permeability measurements in a small membrane reactor set-up, a lumped flux expression for the dead-end Pd-membranes has been developed by Patil et al. [15], summarized in Table 1. The authors have demonstrated that external gas phase mass transfer limitations could be neglected in their flux experiments. Additional experiments were carried out in the pilot plant to determine the membrane permeability for the U-shaped Pd-based membranes. Again, absence of external gas phase mass transfer limitations to the membrane surface was experimentally verified by demonstrating that the membrane flux was only a function of the hydrogen partial pressure and that identical membrane fluxes were measured for cases with pure hydrogen and for cases with a H_2/N_2 mixture with different compositions at different operating pressures, but the same hydrogen partial pressure. Experimental results for the membrane permeability where the

Table 1 Permeation characteristics of the used dead-end and U-shaped Pd-based membranes

Flux of H_2 through Pd membranes			
$J_{H_2} = K_m\left(p^n_{H_2,f} - p^n_{H_2,p}\right)$ where p_{H_2} is the hydrogen partial pressure [Pa] and K_m is the membrane permeance [mol/(m^2 s Pa^n)]			
Dead end Pd membrane			
Pd layer thickness	4.5×10^{-6}		m
Membrane diameter	3		mm
Membrane length	200		mm
U-shaped Pd membrane			
Pd layer thickness	1.5×10^{-6}		m
Membrane diameter	3		mm
Membrane length	410		mm
	T (K)	n	K_m (mol/m^2 s Pa^n)
Permeation results			
Dead end	773	0.9309	8.38×10^{-9}
U-shaped	773	0.9309	4.31×10^{-9}
Dead end	873	0.7836	6.56×10^{-8}
U-shaped	873	0.7836	4.61×10^{-8}

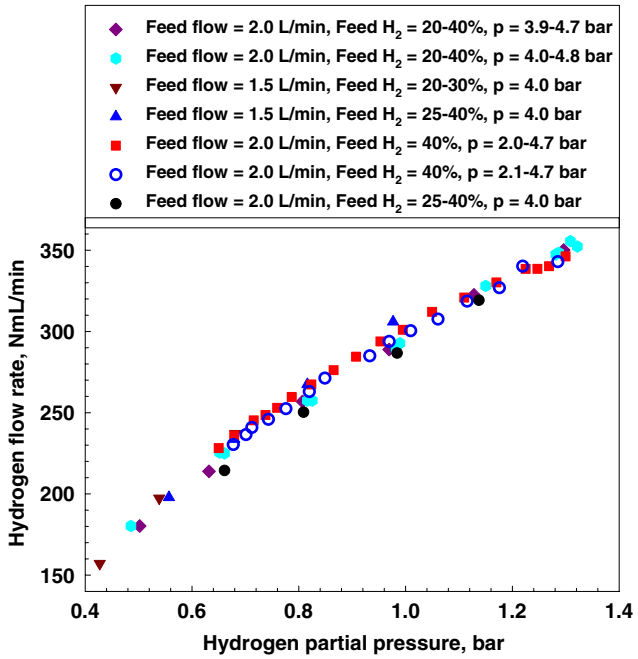

Fig. 4 Hydrogen permeation flow rate through a U-shaped membrane as a function of the hydrogen partial pressure ($T = 600$ °C)

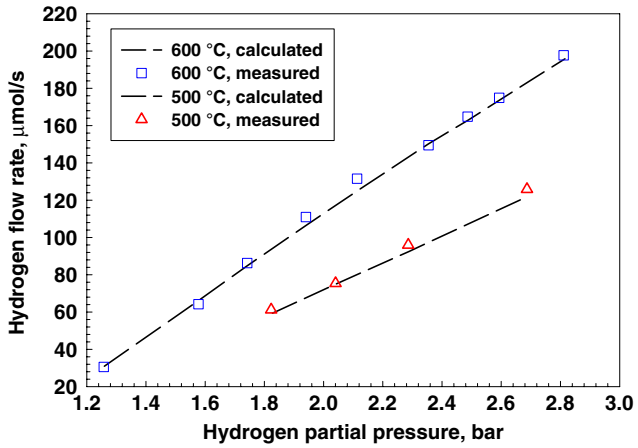

Fig. 5 Comparison of calculated and measured hydrogen flow rate through the U-shaped membrane as a function of the hydrogen partial pressure at two different temperatures

hydrogen partial pressure was varied by varying the composition at the same operating pressure and by varying the pressure for the same composition are shown in Fig. 4. A lumped flux expression for the hydrogen permeability has been derived from the experimental data and is also given in Table 1. In Fig. 5 a comparison between the measured and calculated fluxes as a function of the hydrogen partial pressure at two different temperatures is given, showing good agreement with a maximum error of 4.8%. With the micro-GC it was confirmed that the perm-selectivity (defined as the H_2 flow relative to the flow of the other component) of all other components were well above 10^4.

Next, the reactor performance of the two reactor configurations will be discussed consecutively in terms of the methane conversion (relative change in methane molar flow rate) and the CO selectivity (CO molar flow rate relative to the sum of the CO and CO_2 molar flow rates in the product stream). The measured results will be interpreted with a simplified model, which essentially assumes infinitely very fast reaction kinetics and bubble-to-emulsion phase mass transfer and complete back-mixing in the emulsion phase. For the case of a fluidized bed without membranes, this model reduces to the ideally well-mixed equilibrium reactor. For the fluidized bed membrane reactor concepts, hydrogen extraction from the reaction mixture via the membranes is taken into account with the correlations listed in Table 1. It should be pointed out here that the hydrogen flux through the membranes is somewhat underestimated with this model, due to the fact that the hydrogen partial pressure in the reaction mixture is somewhat underestimated as a consequence of the assumption that the reaction mixture is well-mixed. The validity of the assumptions will be studied with a more detailed model in part 2 of this work.

4.2 Methane Combustion Configuration

First, the performance of a fluidized bed membrane reactor for autothermal reforming of methane is investigated with experiments where methane, steam and air are all fed to a fluidized bed with immersed hydrogen perm-selective membranes in order to demonstrate the technical feasibility of the methane combustion configuration. A typical experiment consists of first determining the feed composition experimentally (using the reactor bypass), then feeding the gaseous reactants to the fluidized bed with permeate sides of the membranes closed and measuring the reactor exhaust composition and finally, measuring the reactor exhaust composition and permeate flow rate for the case that the permeate side of the dead-end membranes was opened and a vacuum was applied. When referring to measurements without the membranes, it should be understood that in these measurements the before-described reactor unit was used with the membrane bundle physically present inside, however, where H_2 was not extracted. A typical example of the measured product composition during an experiment is shown in Fig. 6. The figure clearly shows that the use of Pd membranes positively influences the methane conversion (decrease in methane partial pressure). Moreover, part of the hydrogen produced is recovered as CO-free hydrogen stream, which can be directly fed to a PEM fuel cell. It is highlighted here that no temperature gradients inside the fluidized bed were observed. Experiments were carried out at 600 °C and 2 bara operating pressure for different feed compositions, varying the O_2/

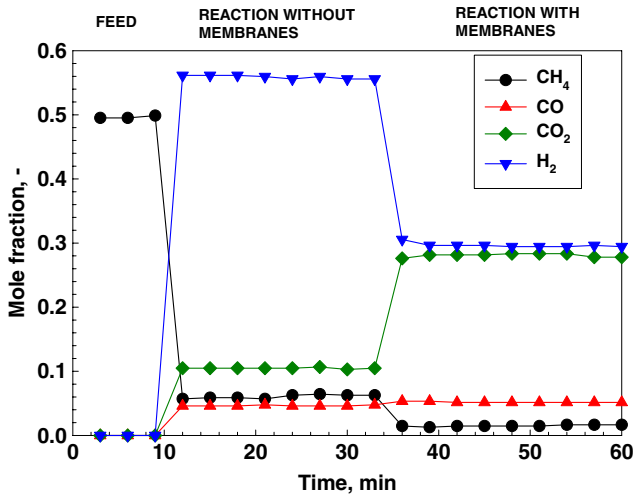

Fig. 6 Feed and product composition as a function of time during a typical experiment

CH_4 ratio in the range 0–0.4 and the H_2O/CH_4 ratio in the range 3–4 and at different gas velocities u/u_{mf} in the range 2–4 (the minimum fluidization velocity u_{mf} was experimentally determined at 2.71×10^{-3} m s^{-1} at 600 °C using pressure drop measurements). In these experiments N_2 was used as a reference inert gas to check the mass balance.

Figure 7 shows that the CH_4 conversion increases and the CO selectivity decreases when increasing the O_2/CH_4 ratio in the feed for both the case with and without membranes, as expected, because of the additional oxidation reactions (*viz.* methane partial oxidation) and consecutive water–gas-shift reaction. The figure also shows the clear benefit of H_2 extraction via the dead-end Pd-membranes, i.e. strong increase in methane conversion and strong decrease in CO selectivity (esp. at high O_2/CH_4 ratios). The simplified reactor model, that assumes infinitely fast reaction kinetics and bubble-to-emulsion phase mass transfer and complete back-mixing, describes the experimental results quite reasonably. The small discrepancies are attributed to small bubble-to-emulsion phase mass transfer limitations or overestimation of the extent of mixing in the emulsion phase, which will be studied in more detail in Part 2 of this work. The total amount of hydrogen produced and the amount of hydrogen extracted via the Pd membranes decreases for increasing O_2/CH_4 ratios, as depicted in Fig. 8a. Due additional oxidation reactions (note that the oxygen conversion was complete in all cases) and consecutive water–gas-shift, the hydrogen partial pressure and consequently the hydrogen permeation rate decreases, decreasing the amount of H_2 produced per mole of CH_4 fed (see Fig. 8b). The underestimation of the amount of hydrogen extracted via the membranes is explained by the overestimation of the axial gas back-mixing in the fluidized bed. The presence of the membranes and the extraction of gas out of the emulsion phase strongly obstruct the macro-

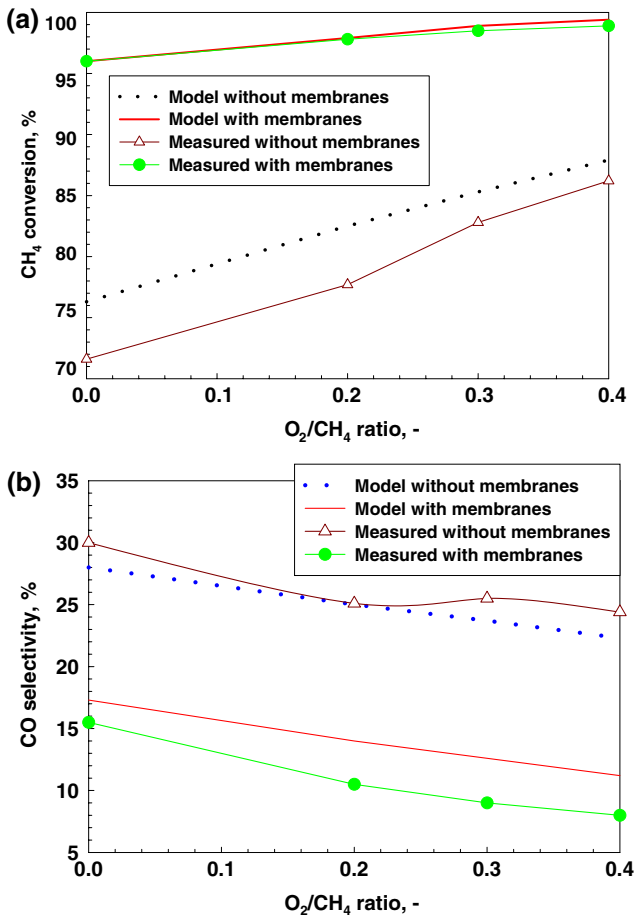

Fig. 7 Measured and calculated CH_4 conversion (**a**) and CO selectivity (**b**) as a function of the O_2/CH_4 ratio in the feed with and without membranes (methane combustion configuration, $T = 600$ °C, $p = 2$ bar, $u/u_{mf} = 2$, $H_2O/CH_4 = 4$, $O_2/CH_4 = 0$–0.4)

scale solids circulation usually present in fluidized beds without internals, resulting in more plug-flow behavior of the gas phase, without destroying the excellent heat transfer characteristics of the fluidized bed (i.e. virtually isothermal conditions) (Deshmukh et al. [24]). In addition, by providing more membrane area (or membranes with a higher hydrogen permeability) the hydrogen production rate could be further increased. From Figs. 7 and 8, it is clear that at higher O_2/CH_4 ratios, the CH_4 conversion increases and the CO selectivity decreases, but with a negative effect on the total H_2 production rate. However, feeding air enables operation under autothermal conditions. How to tune the O_2/CH_4 ratio for overall autothermal operation and what the reactor performance is under these conditions is discussed in Part 2 of this work.

An important parameter influencing the reactor performance is the H_2O/CH_4 feed ratio. In fact, steam is added to the reactor system for the steam reforming and water–gas-shift reactions but also to avoid carbon deposition. In order to investigate the effect of the H_2O/CH_4 ratio on the CH_4

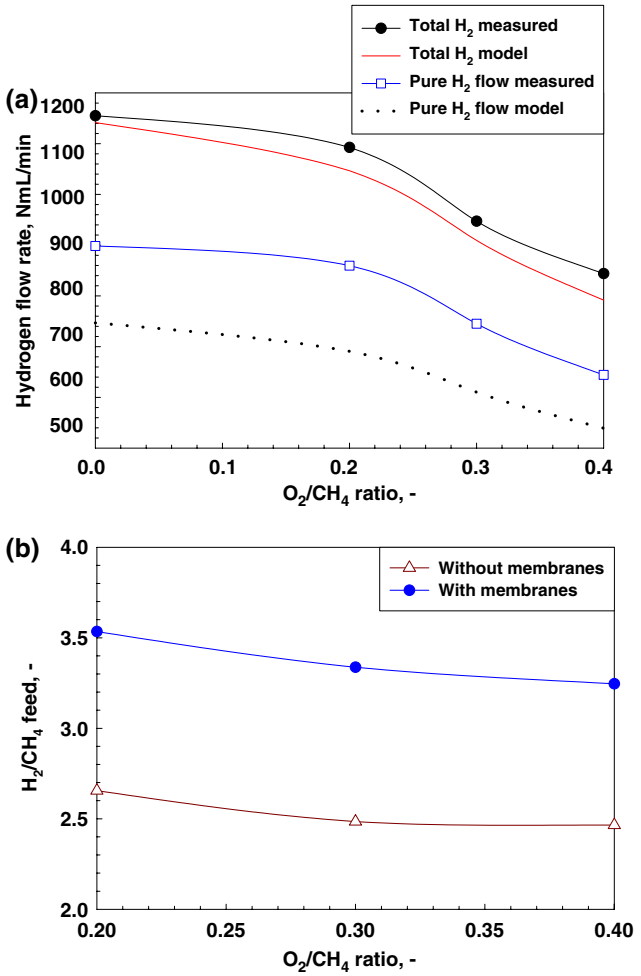

Fig. 8 Measured and calculated total H_2 production and extracted H_2 flow rate (**a**) and H_2 yield (extracted H_2/CH_4 fed) (**b**) as a function of the O_2/CH_4 ratio in the feed (methane combustion configuration, $T = 600$ °C, $p = 2$ bar, $u/u_{mf} = 2$, $H_2O/CH_4 = 4$)

conversion, CO selectivity, H_2 production and H_2 flow, experiments have been carried out for two different H_2O/CH_4 ratios keeping all other conditions identical. The experimental results including predictions with the simplified reactor model are summarized in Table 2. At higher H_2O/CH_4 ratios the CH_4 conversion is somewhat higher and the CO selectivity somewhat lower, as expected due to the shift in the steam reforming and water–gas-shift equilibria, for both the case with and without membranes. However, the total amount of H_2 produced and the total amount of H_2 extracted is slightly lower at higher H_2O/CH_4 ratios, which is related to lower CH_4 inlet concentration when increasing the H_2O/CH_4 ratio at the same fluidization velocity and the correspondingly lower H_2 partial pressure and membrane permeation (Table 3). Nevertheless, the H_2 extracted per mole of CH_4 fed is higher at higher H_2O/CH_4 ratios, pointing at an overall positive effect on the H_2 yield.

Subsequently, the effect of the superficial gas velocity (u/u_{mf}) on the CH_4 conversion, CO selectivity, total H_2 production and total H_2 extracted was investigated in the range of 2–4 (see Figs. 9 and 10). For the case with membranes, the CH_4 conversion decreases and the CO selectivity increases at higher superficial gas velocities, while there is hardly any effect of the throughput on the CH_4 conversion and CO selectivity for the case without membranes. The fact that the superficial gas velocity does not affect the CH_4 conversion for the case without membranes implies no effects of kinetic limitations. The decrease in CH_4 conversion and increase in CO selectivity at higher gas velocities is explained by the fact that the H_2 extraction via the membranes is becoming the limiting factor at higher gas velocities. This can be clearly discerned from Fig. 10a showing that the total amount of H_2 produced increases linearly with the superficial gas velocity, while the amount of H_2 extracted via the membranes levels off to about 1000 Nml/min at u/u_{mf} higher than 3, resulting in a corresponding decrease of the number of moles of H_2 extracted per mole of CH_4 fed (see Fig. 10b). Moreover, for the case with membranes at relatively low superficial gas velocities ($u/u_{mf} = 2$) the prediction with the simplified model for the CH_4 conversion is very close to the experimentally determined CH_4 conversion, while at higher gas velocities the discrepancies become much larger, which indicates the growing importance of bubble-to-emulsion phase mass transfer limitations.

Finally, it can be concluded that autothermal methane reforming can be carried out in a fluidized bed membrane reactor with in situ methane combustion without any problems associated with heat management. Moreover, it

Table 2 The calculated and measured CH_4 conversion and CO selectivity with and without membranes at two different H_2O/CH_4 ratios (methane combustion configuration, $T = 600$ °C, $p = 2$ bar, $u/u_{mf} = 2$, $H_2O/CH_4 = 3$–4, $O_2/CH_4 = 0.2$)

H_2O/CH_4	Model without membranes	Model with membranes	Measured without membranes	Measured with membranes
CH_4 conversion				
3	75.3	95.1	70.4	93.7
4	82.5	97.9	77.7	97.8
CO selectivity				
3	29.3	19.4	29.6	16.0
4	25.1	14.0	25.0	10.5

Table 3 Total H_2 production and extracted H_2 flow rate in membrane reactor and H_2 yield (H_2 extracted/CH_4 fed) at two different H_2O/CH_4 ratios (methane combustion configuration, $T = 600$ °C, $p = 2$ bar, $u/u_{mf} = 2$, $O_2/CH_4 = 0.2$)

H_2O/CH_4	Total H_2 measured	Total H_2 calculated	Extracted H_2 measured	Extracted H_2 calculated
H_2 flow rate (NmL/min)				
3	1225	1191	871	771
4	1092	1046	860	691
H_2O/CH_4	Without membranes		With membranes	
H_2 yield				
3	2.41		3.34	
4	2.66		3.53	

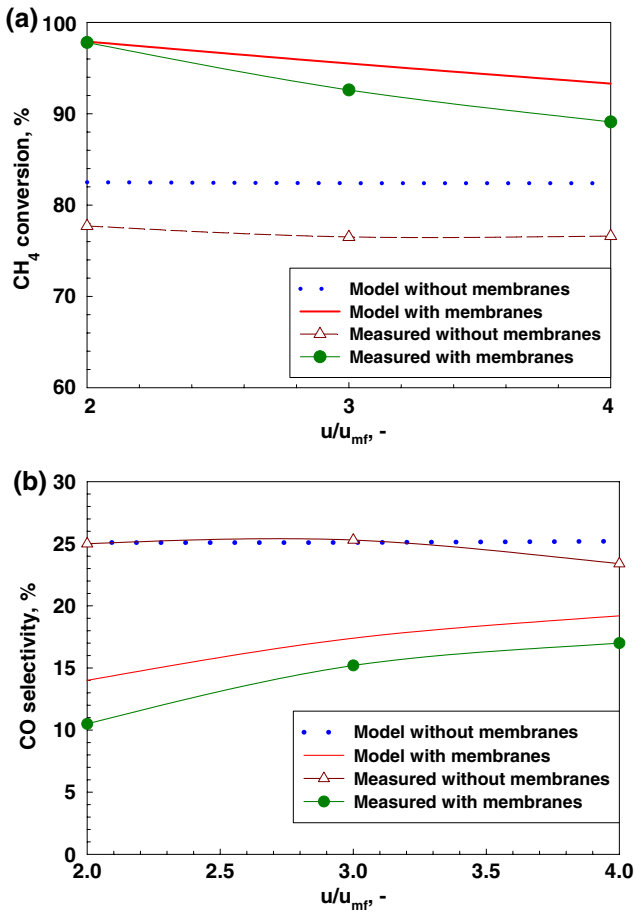

Fig. 9 Measured and calculated CH_4 conversion (**a**) and CO selectivity (**b**) as a function of the relative superficial gas velocity (u/u_{mf}) with and without membranes (methane combustion configuration, $T = 600$ °C, $p = 2$ bar, $u/u_{mf} = 2$–4, $H_2O/CH_4 = 4$, $O_2/CH_4 = 0.2$)

was demonstrated that at relatively low fluidization velocities ($u/u_{mf} \sim 2$), the membrane permeation rate is the limiting factor in the production rate of ultra-pure H_2,

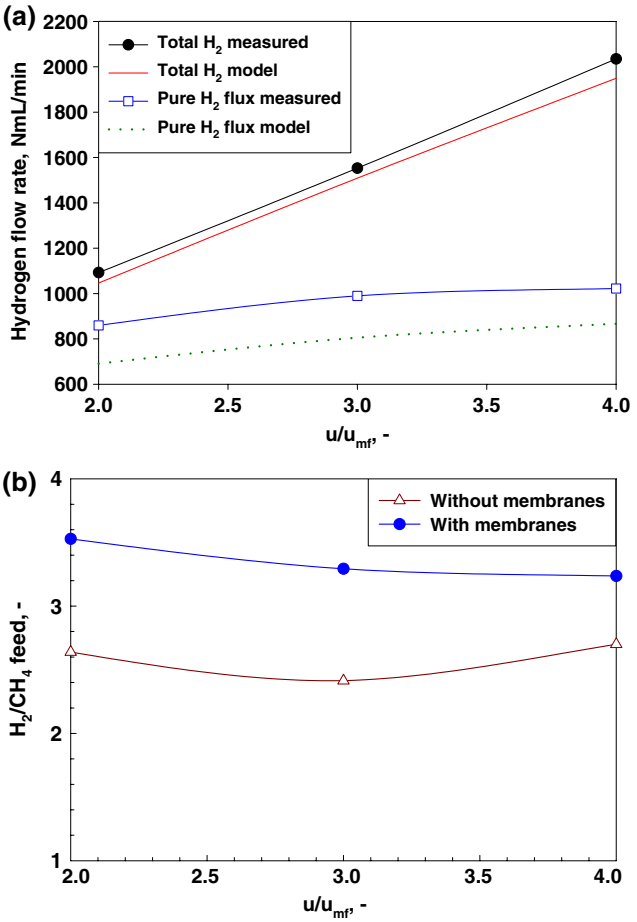

Fig. 10 Measured and calculated total H_2 production and extracted H_2 flow rate (**a**) and H_2 yield (extracted H_2/CH_4 fed) (**b**) as a function of the relative superficial gas velocity (u/u_{mf}) (methane combustion configuration, $T = 600$ °C, $p = 2$ bar, $u/u_{mf} = 2$, $H_2O/CH_4 = 4$, $O_2/CH_4 = 0.2$)

excluding any efficiency losses due to mass transfer limitations from the bed to the membrane surface under these conditions.

4.3 Hydrogen Combustion Configuration

In the hydrogen combustion configuration, the energy required for the endothermic methane steam reforming is supplied by extracting selectively part of the produced H_2 via a U-shaped Pd-membrane immersed in the fluidized bed and combusting the permeated hydrogen with air inside this membrane (also referred to as oxidative sweeping). Note that the Pd layer on the inside of the membrane can act as a catalyst for the hydrogen combustion. First, experiments were carried out to verify the extent of hydrogen combustion inside the U-shaped membranes. Subsequently, the associated temperature increase at the membrane surface due to the hydrogen combustion is

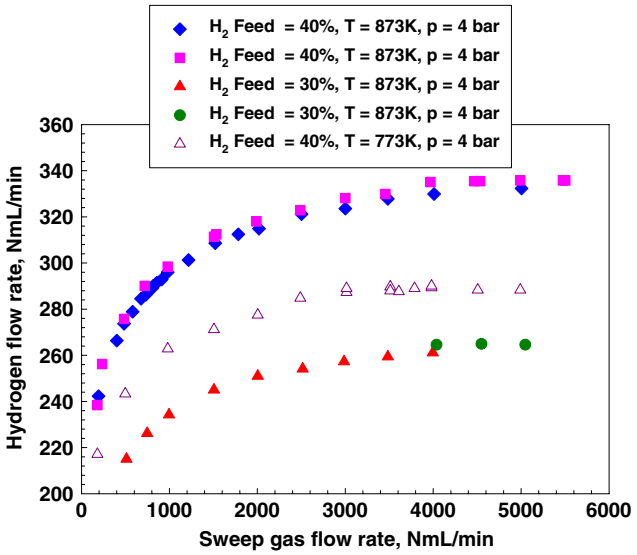

Fig. 11 Hydrogen flow rate permeated through the U-shaped membrane as a function of the inert sweep gas flow rate

discussed. Finally, the results of the reactor tests for the hydrogen combustion configuration are described.

4.3.1 Hydrogen Combustion

First, the minimum sweep gas flow rate (using an inert sweep gas: 99.95% pure N_2) required to reach the maximum hydrogen flow through the U-shaped membrane has been experimentally determined. The experimental results have been summarized in Fig. 11, showing that the permeated hydrogen flow levels off above about 4.5 NL/min for all conditions investigated. This sweep gas flow rate was used in subsequent experiments.

Subsequently, the oxygen concentration in the sweep gas was increased and the O_2 and H_2 conversion was determined. The results for the H_2 flow rate permeated and converted in the U-shape membrane as well as the extent of the O_2 conversion is shown in Figs. 12 and 13 for two different H_2 concentration levels in the feed (5 and 35% H_2 at the retentate side) as a function of the relative amount of O_2 in the sweep gas that is required to combust the permeated H_2 (i.e. $O_2/0.5\ H_2 = 1$ corresponds to complete conversion of both permeated H_2 and O_2 fed). These figures show that a ratio of $O_2/0.5\ H_2$ of about 1.8 is required to achieve full conversion of the permeated H_2, while at $O_2/0.5\ H_2 = 1$ only 78% of the permeated H_2 is converted (for the case of 5% H_2 in the feed to the fluidized bed). When kinetic limitations and/or radial diffusion limitations inside the U-shaped membrane could be reduced, the sweep gas flow rate could in principle be reduced. At higher H_2 content in the feed and thus higher H_2 permeation flow rates, the ratio $O_2/0.5\ H_2$ required for complete H_2 conversion actually decreases (1.6 for 35% H_2

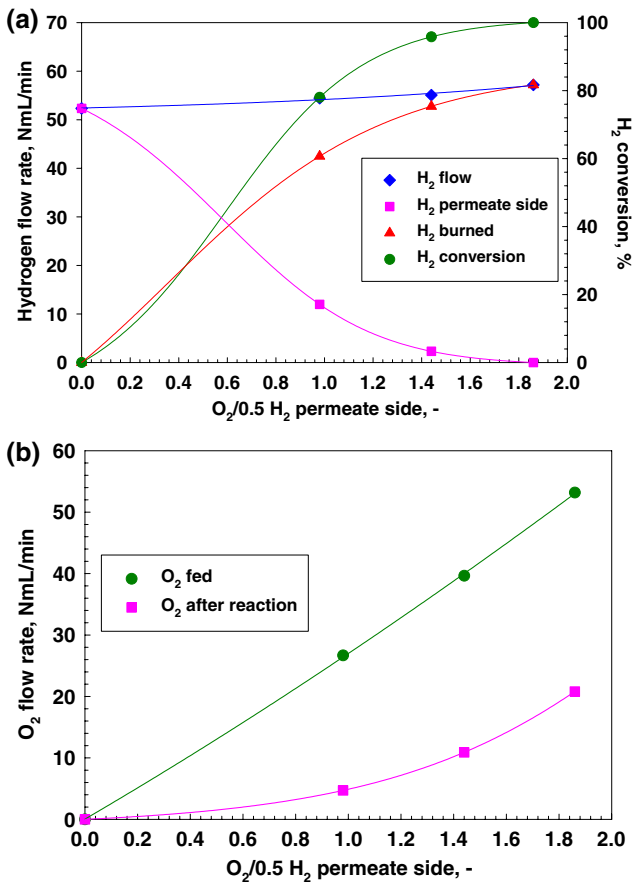

Fig. 12 Results in case of oxidative sweeping for a feed of 5% H_2 at 500 °C ($p = 3$ bar, sweep gas flow rate = 4.5 NL/min)

concentration in the feed), which is most likely related to an increase in the surface temperature (see next section). Concluding, provided that sufficient O_2 is fed to the permeate side of the U-shaped membrane, all the permeated H_2 can be combusted completely, without the requirement of (additional) special catalysts.

4.3.2 Temperature Increase

The combustion of hydrogen inside the U-shaped membrane produces a large amount of energy, which needs to be transferred to the fluidized bed where the endothermic steam reforming of methane is taking place. The temperature increase over the sweep gas side of the membrane has been measured with a thermocouple and has been compared with the calculated maximum temperature increase when all the permeated hydrogen is combusted on the permeate side of the membrane and no energy is transferred back to the fluidized bed (see Table 4). It can be seen that in the case with the 35% H_2 in the feed and complete combustion of the H_2 in the U-shaped membrane, the adiabatic temperature rise is equal to 265 °C, while the measured temperature increase at the outlet of the

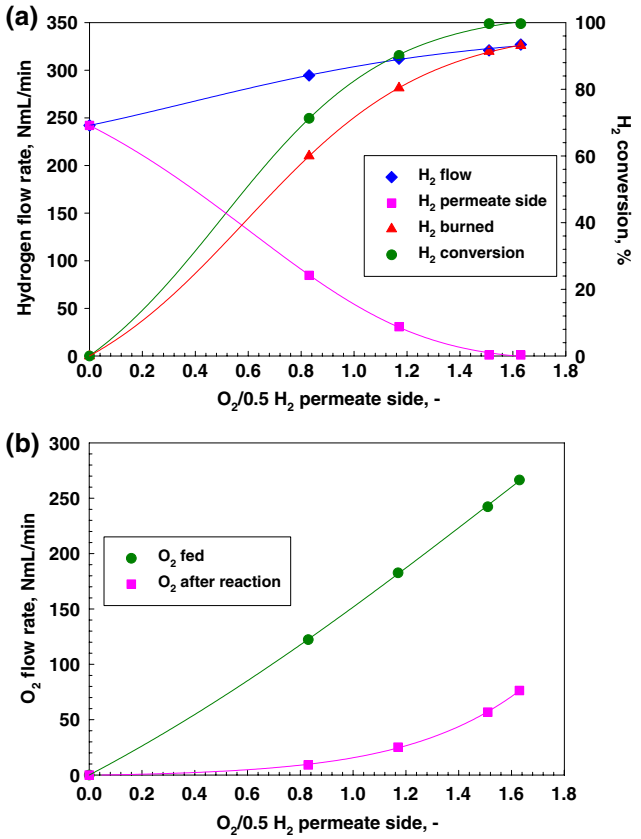

Fig. 13 Results in case of oxidative sweeping for a feed of 35% H_2 at 500 °C ($p = 3$ bar, sweep gas flow rate = 4.5 NL/min)

membrane is only 39 °C. This confirms that indeed most of the heat (>85%) is transferred to the fluidized bed. From these experiments, the overall heat transfer coefficient from the membrane to the fluidized bed can be estimated at 550–600 W m^{-2} K^{-1}, which is indeed much higher than could possibly have been achieved in a packed bed membrane reactor.

4.3.3 Reaction Tests

The technical feasibility of the hydrogen combustion concept was tested with reactive mixtures using the following sequence in the experiments: 1) reaction without membranes; 2) reaction with dead-end and U-shaped membranes using inert N_2 as sweep gas, and 3) reaction with dead-end and U-shaped membranes and oxidative sweep gas (air diluted with N_2). Also in these experiments, N_2 was used as a reference inert gas to check the overall mass balance. In Table 5 the effect of the extraction of H_2 with both dead-end and U-shaped membranes and the combustion of H_2 at the permeate side of the membrane on the CH_4 conversion, CO selectivity, total H_2 production and extracted H_2 flow is presented. The insertion of the dead-end and U-shaped membranes with inert sweep gas

Table 4 Measured temperature increase over the sweep gas as a function of the oxygen concentration in the sweep gas (air diluted with N_2) compared with the calculated adiabatic temperature rise in case of no heat exchange with the fluidized bed

O_2/(0.5 H_2) ratio	$\Delta T_{measured}$ (°C)	ΔT_{ad} (°C)
5% H_2 in feed, $T = 500$ °C, $p = 3$ bar, sweep gas flow rate = 4.5 NmL/min		
0.00	–	–
0.97	5.1	80.3
1.44	7.1	80.1
1.85	8.0	81.6
35% H_2 in feed, $T = 500$ °C, $p = 3$ bar, sweep gas flow rate = 4.5 NmL/min		
0.00	–	–
0.83	17.7	268.6
1.16	30.8	270.0
1.51	38.4	265.5
1.63	39.2	265.2

results in a higher CH_4 conversion, lower CO selectivity and higher H_2 production due to the shift in the steam reforming and water–gas-shift reactions. Interestingly, when using oxidative sweeping in the U-shaped membranes, the performance further improves (even higher CH_4 conversion, lower CO selectivity and higher H_2 production and H_2 extraction and higher H_2 yield). This is attributed to the higher membrane temperature as a result of the hydrogen combustion in case of oxidative sweeping, increasing the membrane permeability.

The effect of the H_2O/CH_4 ratio on the reactor performance when using oxidative sweeping in the U-shaped membrane is investigated. The results are summarized in Table 6, showing that the CH_4 conversion increases and the CO selectivity decreases from with increasing H_2O/CH_4 ratio, due to the shift in the steam reforming and water–gas-shift reactions. From Table 6 it can be discerned that the membrane reactor gives an increase in the CH_4 conversion of 76% at H_2O/CH_4 ratio = 3 and 69% at H_2O/CH_4 ratio = 4, while the CO selectivity decreases with 38% at H_2O/CH_4 ratio = 3 and with 46% at H_2O/CH_4 ratio = 4, in comparison to a reactor without membranes. Despite the higher conversion and lower CO selectivity, the hydrogen production only slightly increases (see Table 7), since the additional shift is counterbalanced by the higher dilution of the feed at higher steam ratios.

Finally, it can be concluded that overall autothermal steam reforming can also be carried out in a fluidized bed membrane reactor with hydrogen combustion without any problems associated with heat management. It has been shown that it is possible to combust the permeated hydrogen inside the Pd membrane (without additional catalyst) and to transfer the energy produced back to the fluidized bed.

Table 5 Effect of H_2 combustion on the CH_4 conversion, CO selectivity, total H_2 production and extracted H_2 flow rate, and H_2 yield (H_2 extracted/CH_4 fed) (hydrogen combustion configuration, $T = 500$ °C, $p = 2$ bar, $N_2/CH_4 = 2$, $H_2O/CH_4 = 4$)

Experimental step	CH_4 conversion	CO selectivity	H_2 production (NmL/min)	H_2 flow (NmL/min)	H_2/CH_4 feed
1	43.9	11.85	583	500	1.76
2	68.5	6.52	888	661	2.70
3	74.6	6.44	958	749	2.92

Table 6 CH_4 conversion and CO selectivity with and without membranes for two different H_2O/CH_4 feed ratios (hydrogen combustion configuration, $T = 500$ °C, $p = 3$ bar, $N_2/CH_4 = 2$)

H_2O/CH_4	With membranes		Without membranes	
	CH_4 conversion	CO selectivity	CH_4 conversion	CO selectivity
3	63.3	8.2	35.8	13.3
4	74.2	6.4	43.9	11.9

Table 7 H_2 production and flow rates through the membranes (hydrogen combustion configuration, $T = 500$ °C, $p = 3$ bar, $N_2/CH_4 = 2$, $u/u_{mf} = 2$)

	$H_2O/CH_4 = 3$	$H_2O/CH_4 = 4$
Total H_2 production (NmL/min)	869	887
Total H_2 flow (NmL/min)	652	660
H_2 flow dead end membranes (NmL/min)	526	530
H_2 flow U shape membranes (NmL/min)	126	130
Total H_2 flow/total H_2 production	75.0	74.4

5 Conclusions

The technical feasibility of two fluidized bed membrane reactor concepts for the autothermal reforming of methane with integrated CO_2 capture (referred to as the methane combustion and hydrogen combustion configuration) has been demonstrated experimentally. With both membrane reactor concepts, methane conversions beyond equilibrium conversions limiting conventional reactors can be achieved, while simultaneously ultra-pure hydrogen is recovered directly. A more detailed comparison of the performance of the two proposed reactor concepts is carried out with a simulation study and is presented in the second part of this work.

Acknowledgements The authors are grateful to the Dutch Ministry of Economic affairs for financial support of this work in the EOS program (project EOSLT05010).

References

1. Rostrup-Nielsen JR (1984) Catalytic steam reforming. In: Anderson JR, Boudart M (eds) Catalysis science and technology, vol 5. Springer, Berlin
2. Rostrup-Nielsen JR (2002) Syngas in perspective. Catal Today 71(3–4):243–247
3. Adris AM, Elnashaie SSEH, Hughes R (1991) Fluidized bed membrane reactor for the steam reforming of methane. Can J Chem Eng 69(5):1061–1070
4. Kikuchi E (1995) Palladium/ceramic membranes for selective hydrogen permeation and their application to membrane reactor. Catal Today 25(3–4):333–337
5. Oklany JS, Hou K, Hughes R (1998) A simulative comparison of dense and microporous membrane reactors for the steam reforming of methane. Appl Catal A: Gen 170:13–22
6. Shu J, Grandjean BPA, Kaliaguine S (1994) Methane steam reforming in asymmetric Pd- and Pd-Ag/porous SS membrane reactors. Appl Catal A: Gen 119:305–325
7. Gallucci F, Paturzo L, Famà A, Basile A (2004) Experimental study of the methane steam reforming reaction in a dense Pd/Ag membrane reactor. Ind Eng Chem Res 43:928–933
8. Kikuchi E, Uemiya S, Matsuda T (1991) Hydrogen Production from methane steam reforming assisted by use of membrane reactor. Stud Surf Sci Catal 61:509
9. Chai M, Machida M, Eguchi K, Arai H (1993) Promotion of methane steam reforming using tuthenium-dispersed microporous alumina membrane reactor. Chem Lett 41
10. Nam SW, Yoon SP, Ha HY, Hong S-A, Maganyuk AP (2000) Methane steam reforming in a Pd-Ru membrane reactor. Korean J Chem Eng 17(3):288
11. Jarosch K, de Lasa HI (1999) Novel riser simulator for methane reforming using high temperature membranes. Chem Eng Sci 54:1455
12. Gallucci F, Paturzo L, Basile A (2004) A simulation study of the steam reforming of methane in a dense tubular membrane reactor. Int J Hydrogen Energy 29:611–617
13. Hoang DL, Chan SH (2004) Modeling of a catalytic autothermal methane reformer for fuel cell applications. Appl Catal A: Gen 268(1–2):207–216
14. Lattner JR, Harold MP (2004) Comparison of conventional and membrane reactor fuel processors for hydrocarbon-based PEM fuel cell systems. Int J Hydrogen Energy 29(4):393–417
15. Patil CS, van Sint Annaland M, Kuipers JAM (2007) Fluidised bed membrane reactor for ultrapure hydrogen production via methane steam reforming: Experimental demonstration and model validation. Chem Eng Sci 62(11):2989–3007
16. Tiemersma TP, Patil CS, van Sint Annaland M, Kuipers JAM (2006) Modelling of packed bed membrane reactors for autothermal production of ultrapure hydrogen. Chem Eng Sci 61(5):1602–1616
17. De Smet CRH, de Croon MHJM, Berger RJ, Marin GB, Schouten JC (2001) Design of adiabatic fixed-bed reactors for the partial oxidation of methane to synthesis gas, application to production

of methanol and hydrogen-for-fuel-cells. Chem Eng Sci 56(16):4849–4861
18. Ioannides T, Verykios XE (1998) Development of a novel heat-integrated wall reactor for the partial oxidation of methane to synthesis gas. Catal Today 46(2–3):71–81
19. De Groote AM, Froment GF (1996) Simulation of the catalytic partial oxidation of methane to synthesis gas. Appl Catal A: Gen 138(2):245–264
20. Boyd T, Grace J, Lim CJ, Adris AEM (2005) Hydrogen from an internally circulating fluidized bed membrane reactor. Int J Chem Reactor Eng 3(A58):1–10
21. Abashar MEE, Elnashaie SSEH (2007) Feeding of oxygen along the height of a circulating fast fluidized bed membrane reactor for efficient production of hydrogen. Chem Eng Res Des 85(A11): 1529–1538
22. Chen Z, Grace JR, Lim CJ, Li A (2007) Experimental studies of pure hydrogen production in a commercialized fluidized-bed membrane reactor with SMR and ATR catalysts. Int J Hydrogen Energy 32:2359–2366
23. Patil CS (2005) Membrane reactor technology for ultrapure hydrogen production. PhD thesis, University of Twente, The Netherlands. ISBN 90–365-2246-3
24. Deshmukh SARK, Laverman JA, Cents AHG, van Sint Annaland M, Kuipers JAM (2005) Development of a membrane assisted fluidised bed reactor 1. Gas phase back mixing and bubble to emulsion phase mass transfer using tracer injection and ultra-sound experiments. Ind Eng Chem Res 44:5955–5965